crystals

MDPI

Article

Electrical and Optical Characterization of Graphene Oxide and Reduced Graphene Oxide Thin Films

Grazia Giuseppina Politano [1,*] and Carlo Versace [1,2]

[1] Dipartimento di Fisica, Università della Calabria, 87036 Rende, CS, Italy
[2] Licryl CNR/Nanotec c/o Dipartimento di Fisica, Università della Calabria, 87036 Rende, CS, Italy
* Correspondence: grazia.politano@unical.it

Abstract: Despite a growing interest in graphene, an aspect which is less studied is the electrical and optical characterization of graphene oxide (GO)-based transparent conductors obtained using thermal annealing. In addition, few research works have studied the electrical properties of GO and reduced graphene oxide (RGO) films using electrical impedance measurements. In this study, electric impedance measurements are performed on GO and thermally reduced GO films dip-coated on glass substrates. The electric resistance of RGO films decreases by about two orders of magnitude compared to GO films. Moreover, optical microscopy and variable angle spectroscopic ellipsometry (VASE) were carried out on the same samples. Thermal annealing increases the optical conductivity and the absorption coefficient of GO films. Such findings could be used in many optoelectronic applications, improving future GO applicability.

Keywords: graphene oxide; reduced graphene oxide; optical properties; electrical properties; films

Citation: Politano, G.G.; Versace, C. Electrical and Optical Characterization of Graphene Oxide and Reduced Graphene Oxide Thin Films. *Crystals* **2022**, *12*, 1312. https://doi.org/10.3390/cryst12091312

Academic Editor: Qing Peng

Received: 23 August 2022
Accepted: 15 September 2022
Published: 17 September 2022

1. Introduction

The outstanding properties of graphene-based materials are compelling for several applications [1–23]. We investigated the graphene-based films' optical properties in our previous works [24–29].

The study of the electric properties of graphene-based materials opens new possibilities for solid state electronics and for composite materials [30].

Although the result of weak disorder on the electrical conductivity of a single graphene sheet has been widely investigated [31,32], there are not a lot of research works regarding the conductivity of a disordered graphene-based material, such as graphene oxide (GO). GO is insulating because of the breaking of the conjugated electronic structure by means of oxidized functional groups, and it contains permanent defects and disorders [33]. Hence, the electrical properties of GO sheets are dissimilar from those of pristine graphene. The insulating GO films have resistance values higher than about 10^{10} Ω/sq due to their reduced carrier mobility [34]. The reduction in GO is the key to re-establishing the excellent electrical conductivity of graphene. The attached oxygen-containing groups and lattice defects change the GO electronic structure and are scattering centers that influence electrical transport. Consequently, GO reduction aims to remove the oxygen-containing groups and to recover the conjugated network of the graphitic lattice [35], allowing the retrieval of the electrical conductivity of graphene [36].

Even though most of the oxidized groups are suppressed during the reduction process, the residual ones may restrict reduced graphene oxide (RGO) electron transport properties.

Thus, GO reduction restores the conductivity at orders of magnitude values below that of pristine graphene [37]. RGO conductivity varies from 0.05 S/cm to 500 S/cm based on the degree of reduction, which is associated with the ratio of the graphitic regions (sp^2) to the oxidized regions (sp^3) [38,39].

Chemical and thermal reduction are two main methods of GO reduction [40]. Another method of GO reduction is the use of broadband visible light [41].

Reducing GO by using chemical reduction is a very scalable method. Unfortunately, this method uses ecologically harmful reagents, such as hydrazine and hydrazine hydrate [42]. Thus, there is a need to study other low-cost and environmentally friendly GO reduction methods.

Thermal reduction is non-toxic, environmental friendly and ideal for large-scale industrial applications [42]. The thermal reduction in GO is typically achieved above 200 °C and is successful at higher temperatures [43].

GO-based transparent conductors have more defects with lower electrical conductivity, but they may be promising for mass production because of their low cost. Nevertheless, many challenges are still ahead, e.g., the relatively low conductivity, before full-scale industrial application of these materials is possible.

The research on the reduction in GO films using thermal annealing may facilitate its application in optoelectronic devices. Indeed, GO and RGO find several applications in optoelectronic devices, such as perovskite solar cells and photodetectors [44–47].

Various work on the electrical and optical properties of GO and RGO has already been published [48]. However, research on the electrical and optical characterization of RGO films obtained with thermal annealing is less explored [49] in comparison to other reduction methods, such as chemical reduction [50] and UV reduction [51]. Moreover, few research works study the electrical properties of GO and RGO films using electrical impedance measurements, according to our knowledge. Our work wants to fill this gap.

Therefore, the aim of this work is to characterize GO and thermally reduced GO films deposited on glass substrates, using optical microscopy, impedance spectroscopy and variable angle spectroscopic ellipsometry (VASE) measurements [52].

2. Materials and Methods

2.1. Synthesis and Thermal Reduction in GO Films

Corning glass substrates were washed using a mix of sulfuric acid (H_2SO_4) and hydrogen peroxide (H_2O_2), known as "piranha solution".

The samples were produced using 12 mg of GO (Sigma Aldrich, St. Louis, MO, USA), 3 mL of double distilled H_2O and 3 mL of methanol (Sigma Aldrich, St. Louis, MO, USA).

The dip-coating process [53] was used to deposit GO thin films on glass substrates with a homemade apparatus at a speed of 1 mm/min.

GO films on glass substrates were then heated at 450 °C for 20 min in an Ar atmosphere furnace.

2.2. Characterization of GO and RGO Films

Optical microscopy images of the samples were acquired with a Zeiss Axioskop (Zeiss, Oberkochen, Germany).

The electrical impedance measurements were performed using a 4294 Precision Impedance Analyzer (Agilent, Santa Clara, CA, USA) with a 42941A pin probe kit that permits measurements in the range 40 Hz–30 MHz. The measurements were performed by using two close (about 1 mm) gold-tipped electrodes.

The optical conductivity of the films was studied using the VASE technique.

Spectra of the ellipsometric angles ψ and Δ were obtained using a M2000 F (Woollam Co., Lincoln, NE, USA) ellipsometer (Rotating Compensator Ellipsometer) in the (1.2–4.1) eV photon energy range. The data were obtained at 50°, 60° and 70° incident angles (room temperature).

The optical model and the best fitting values were determined with the WVASE32 (J.A. Woollam) application, which uses the nonlinear Levenberg–Marquardt algorithm [54] to determine the minimum value of the mean squared error (MSE) [55].

In Scheme 1, the schematic diagram of the synthesis process is reported.

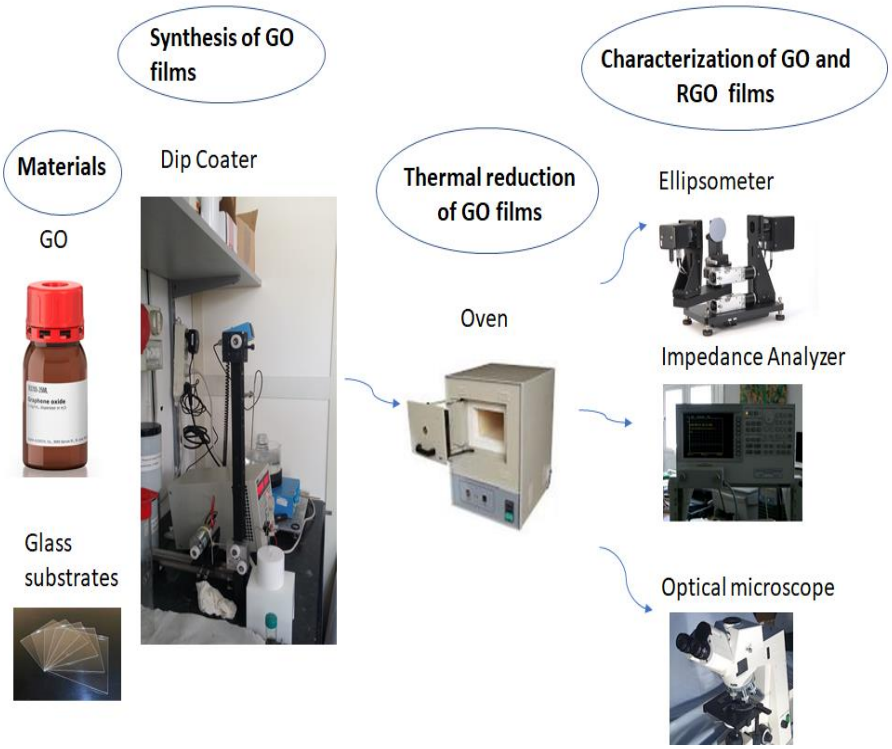

Scheme 1. Schematic diagram of the synthesis process.

3. Results and Discussion

3.1. Optical Microscopy Images

In Figure 1, the optical microscopy images of GO and RGO films after thermal annealing are reported.

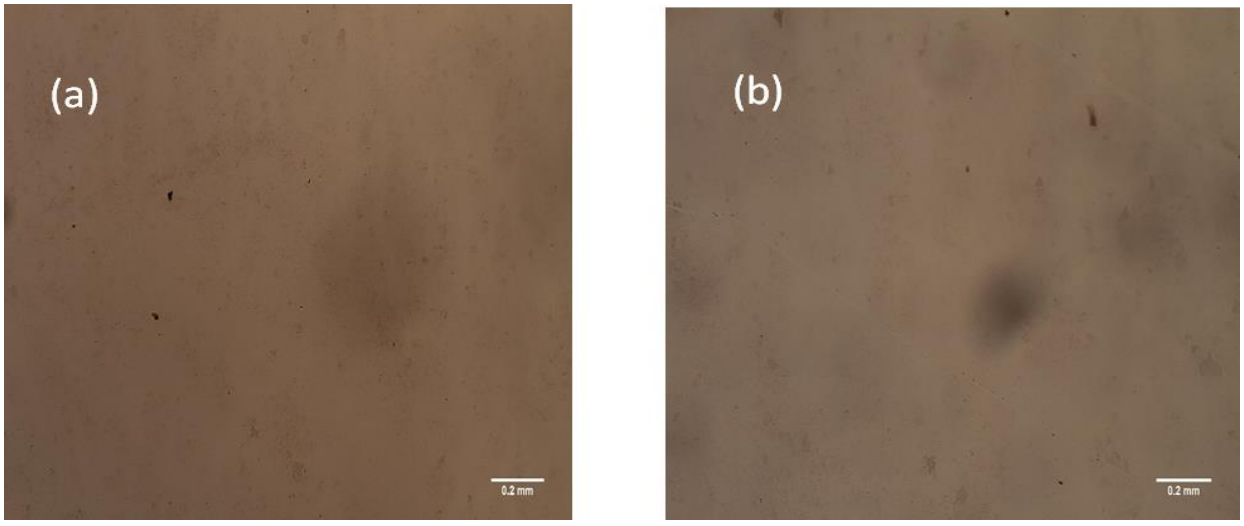

Figure 1. (**a**) Optical microscopy images of GO and (**b**) RGO films after thermal annealing.

Optical observation is an immediate way to see the modifications in GO films before and after thermal annealing. The color transition of GO films from dark yellow (Figure 1a) to black in the initial reduction stage (Figure 1b) is confirmed by optical microscopy images [56]. When GO was reduced, the absorption coefficient increased (see Figure 11). This high absorption coefficient is in accordance with the films becoming black, i.e., the films absorbed light at all wavelengths. Additional morphological analysis of the samples is available in the Supplementary Materials.

3.2. Impedance Measurements

Figure 2 shows the electrical impedance of GO and RGO films on glass (modulus and phase).

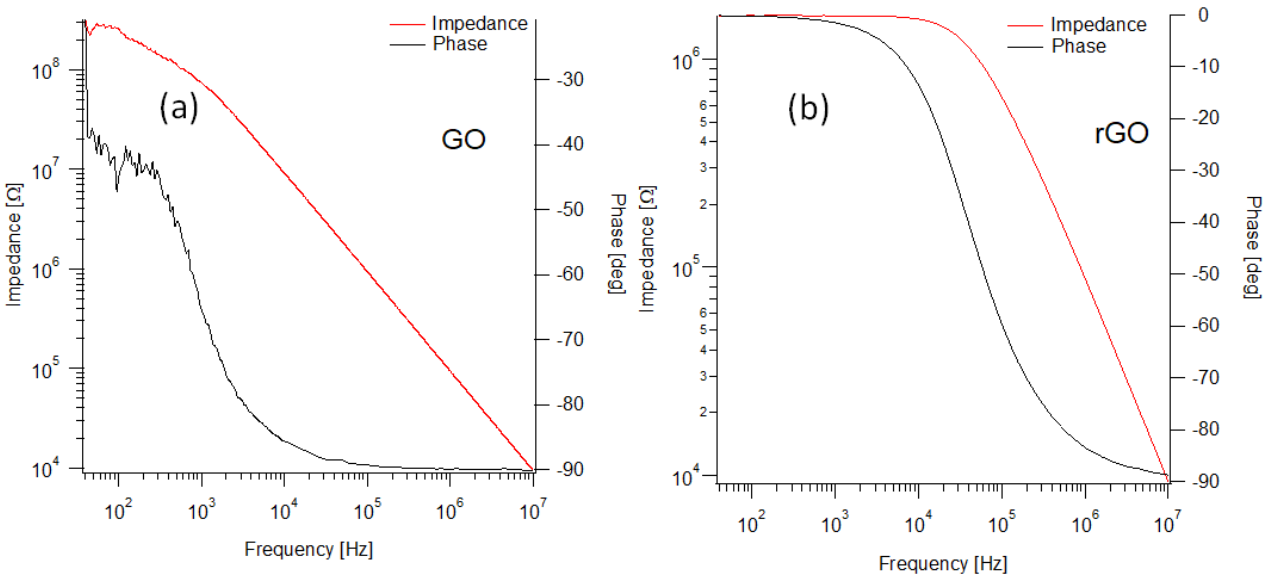

Figure 2. (**a**) Impedance and phase of GO films and (**b**) RGO films on glass substrates.

We noticed that, after the annealing treatment, the resistance of the film declined by about two orders of magnitude, although not uniformly.

As a comparison, the electrical impedance (modulus and phase) of a commercial CVD-grown monolayer graphene on the SiO_2/Si substrate (Graphenea, San Sebastián, Spain) is reported in Figure 3, in which it is possible to observe similar behavior as in RGO films.

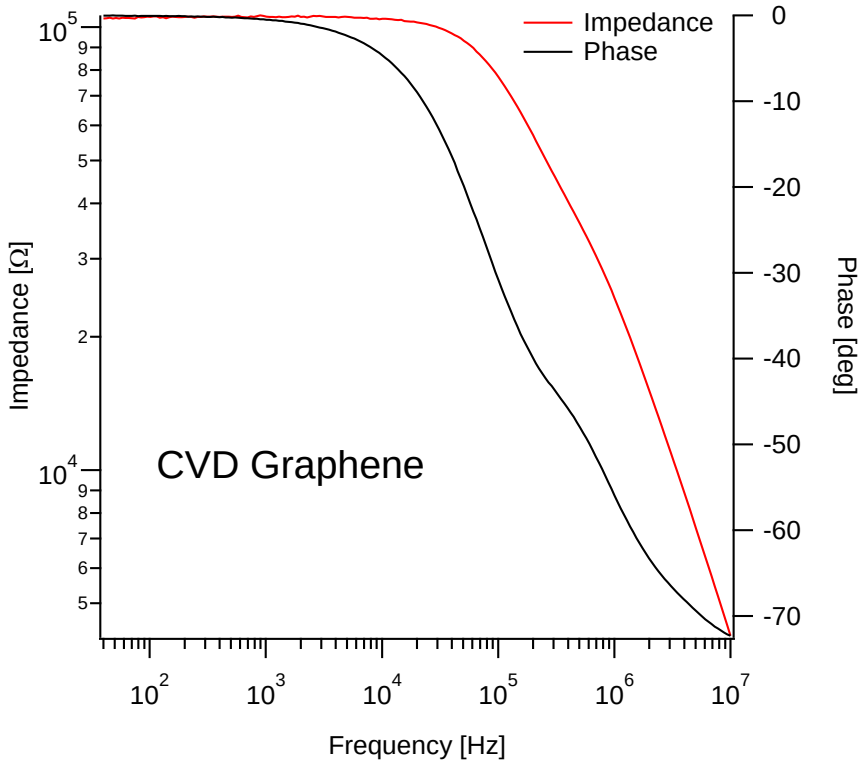

Figure 3. Impedance and phase of CVD-grown monolayer graphene on SiO_2/Si substrate.

3.3. Variable Angle Spectroscopic Ellipsometry Measurements

First, we examined the bare glass substrates by VASE measurements.

Glass substrates were described using a Cauchy–Urbach model [55].

GO and RGO films on glass substrates were modeled as the sum of Lorentz oscillators. The complex dielectric function is described with the following relation [55]:

$$\widetilde{\varepsilon}(h\upsilon) = \varepsilon_1 + i\varepsilon_2 = \varepsilon_\infty + \sum_{k=1}^{N} \frac{A_k}{{E_k}^2 - E^2 - i\Gamma_k E} \quad (1)$$

where E is the incident photons energy, ε_∞ is the real part of the dielectric function when $E \to \infty$, A_k is the amplitude (eV^2), Γ_k is the broadening (eV) end and E_k (eV) is the central energy of the k-th oscillator.

Table 1 shows the parameters obtained from the best fit values of GO and RGO films on glass substrates.

Table 1. Lorenz oscillators parameters for GO and RGO films on glass substrates. Amplitude A_k has unit of eV^2, center energy E_k and broadening Γ_k have units of eV, d is the thickness of film in nm, the frequency dielectric constant ε_∞ is dimensionless.

	GO/Glass	RGO/Glass
d (nm)	38.5 ± 1.1	38 ± 1
ε_∞	2.47 ± 0.04	1.94 ± 0.04
A_1 (eV^2)	7.6 ± 2.5	9.9 ± 3.8
Γ_1 (eV)	1.8 ± 0.1	11.3 ± 1.7
E_1 (eV)	4.7 ± 0.1	4.0 ± 0.3
A_2 (eV^2)	6.8 ± 2.9	38.59 ± 8.2
Γ_2 (eV)	0.0010 ± 0.0001	66.82 ± 5.3
E_2 (eV)	5.1 ± 0.2	4.6 ± 0.1

The models provide outstanding data fittings (MSE ~8).

As we can see from Table 1, we found the π^* peak of plasma excitation at 4.7 eV [50] for the GO films.

After the annealing treatment, the quantity of oxygen decreased, a transition from sp^3 to sp^2 hybridization happened and the absorbance peak showed a red shift [57]. The reduction process caused a variation in the coverage of functional groups, thus changing the RGO [50] electronic density of states.

The red shift of the absorption peak from 5.1 eV (for GO films) to 4.6 eV (for RGO films) was due to an excitonic effect [50].

The complex dielectric constants for GO and RGO films on glass derived from the analysis of VASE measurement are shown in Figures 4 and 5, respectively.

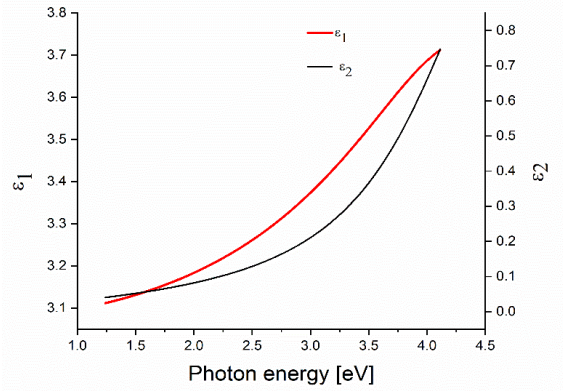

Figure 4. Estimated dispersion laws of GO films on glass substrates by ellipsometry characterization. The solid curves represent the real (red curve) and the imaginary (black curve) part of the dielectric constant.

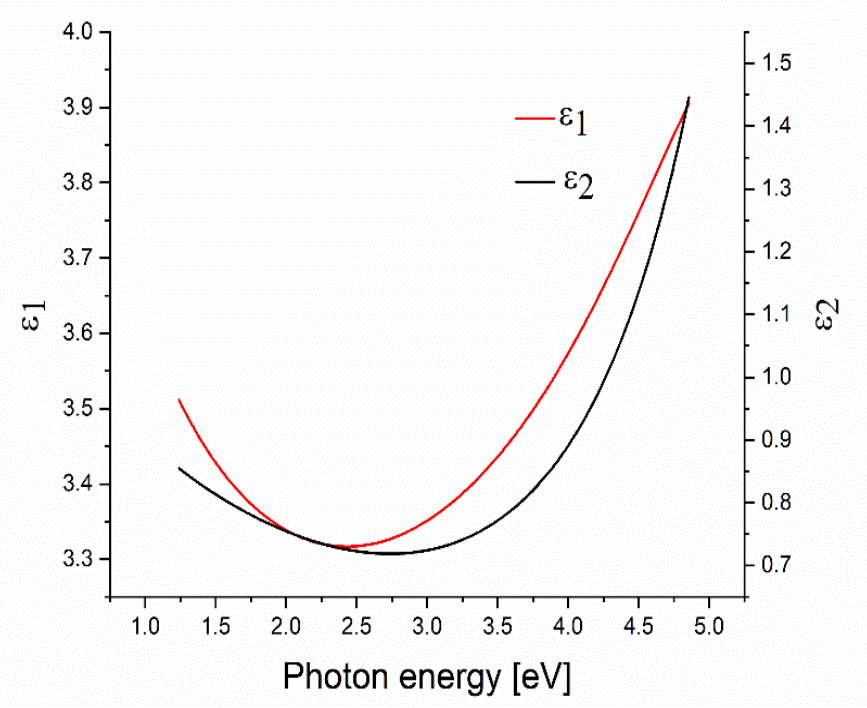

Figure 5. Estimated dispersion laws of RGO films on glass substrates by ellipsometry characterization. The solid curves represent the real (red curve) and the imaginary (black curve) part of the dielectric constant.

Moreover, the refractive index and the extinction coefficient of GO and RGO films are reported in Figures 6 and 7, respectively.

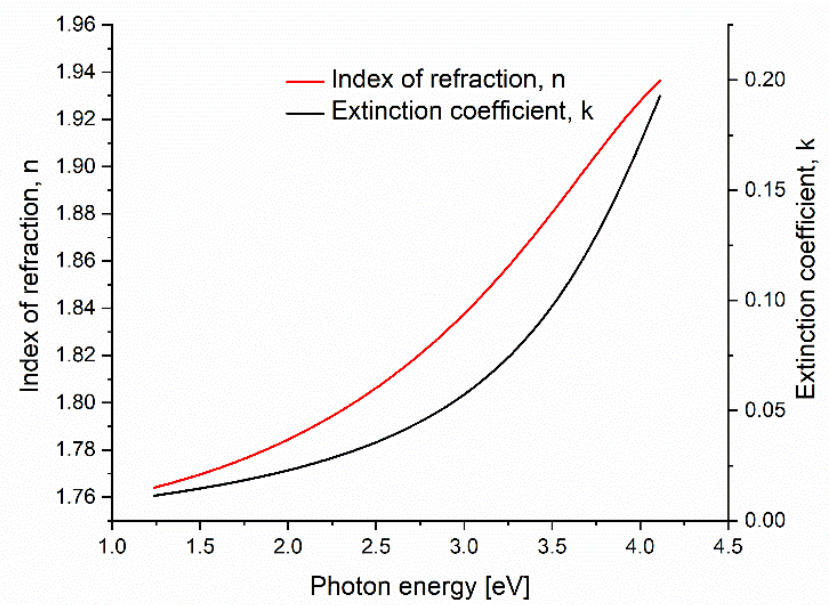

Figure 6. Estimated dispersion laws of GO films on glass substrates by ellipsometry characterization. The curves represent the index of refraction (red curve) and the extinction coefficient (black curve).

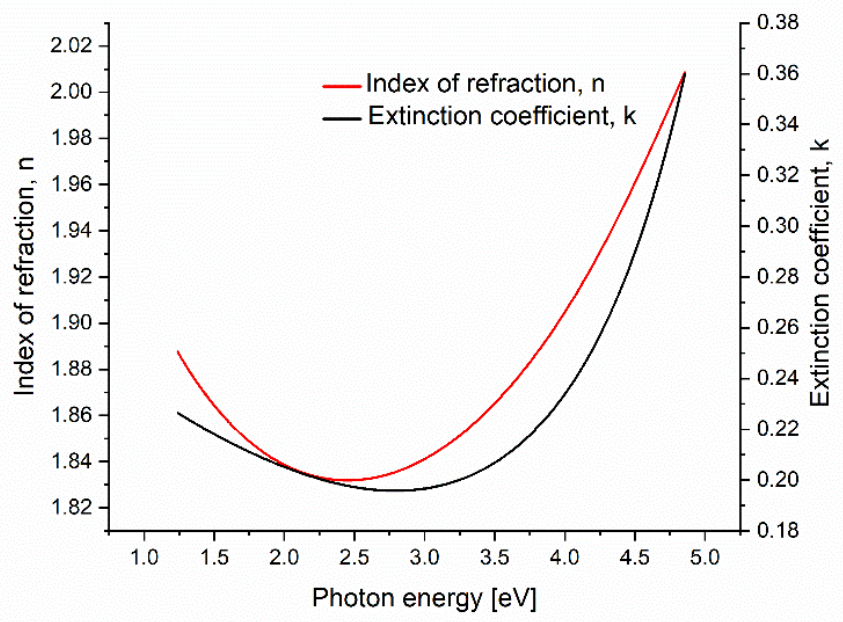

Figure 7. Estimated dispersion laws of RGO films on glass substrates by ellipsometry characterization. The curves represent the index of refraction (red curve) and the extinction coefficient (black curve).

These measurements show an increase in the values of the index of refraction and the extinction coefficient of GO films after the annealing, in accordance with the work of Jung et al. [49].

The complex optical conductivity $\sigma = \sigma_1 + \sigma_2$ is connected to the complex dielectric constant $\varepsilon = \varepsilon_1 + \varepsilon_2$ by the following relations [58]:

$$\sigma_1 = \omega\varepsilon_2\varepsilon_0 \quad \text{and} \quad \sigma_2 = \omega\varepsilon_1\varepsilon_0 \tag{2}$$

where ω is the angular frequency and ε_0 is the free space dielectric constant.

The optical conductivities of GO and RGO films on glass substrates are reported in Figures 8 and 9, respectively. Thermal annealing increased the optical conductivity of GO by about one order of magnitude.

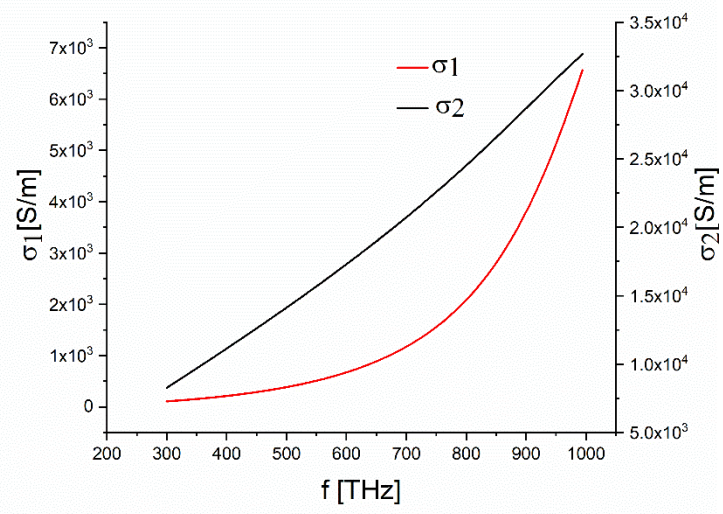

Figure 8. The optical conductivity dependence on frequency of GO films on glass substrates.

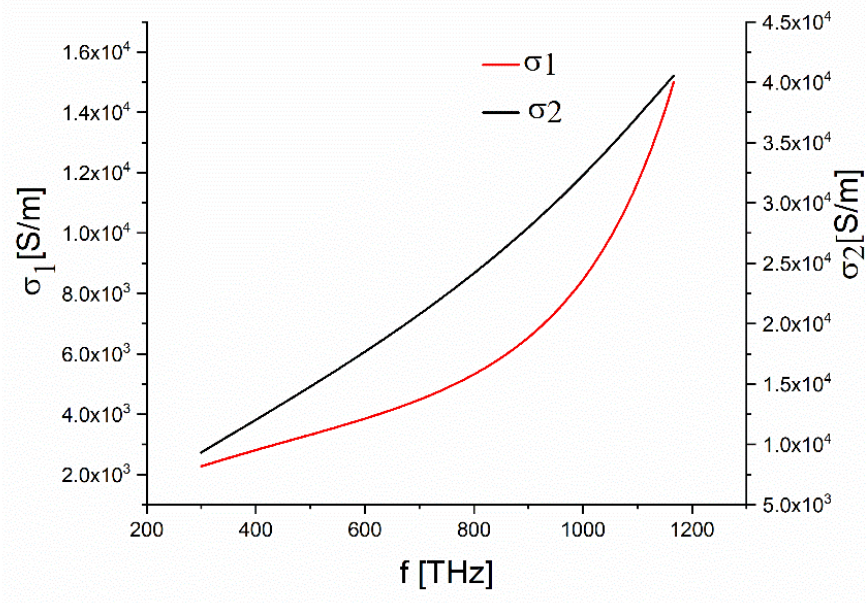

Figure 9. The optical conductivity dependence on frequency of RGO films on glass substrates.

The absorption coefficient is calculated from the estimated extinction coefficient $k(h\nu)$:

$$\alpha(h\nu) = \frac{4\pi\, k(h\nu)}{\lambda} \tag{3}$$

where $h\nu$ and λ are the energy and wavelength of the light, respectively.

Figures 10 and 11 show the absorption coefficient against $h\nu$ photon energy for GO and RGO films, respectively. Thermal annealing increases the absorption coefficient of GO films, as is visible in Figure 11.

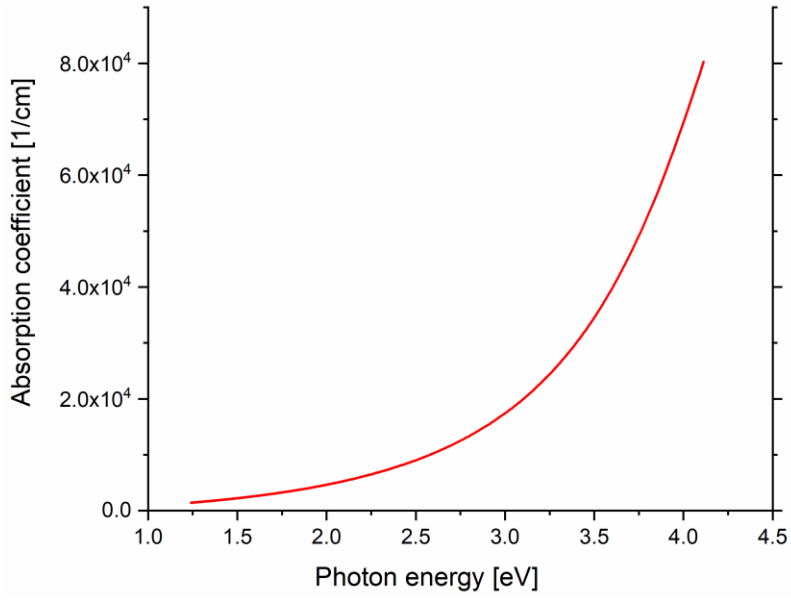

Figure 10. Absorption coefficient against photon energy for GO films.

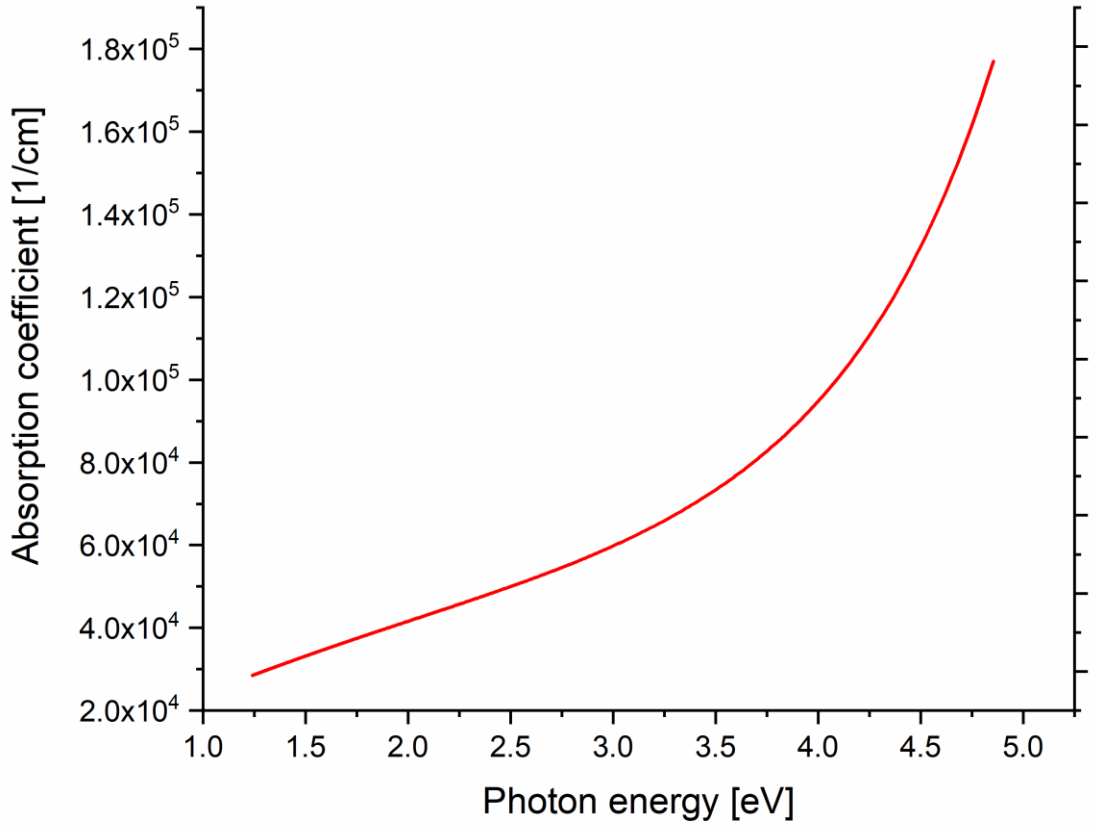

Figure 11. Absorption coefficient against photon energy for RGO films.

4. Conclusions

Herein, we investigated the properties of GO and thermally reduced GO (RGO) thin films dip-coated on glass substrates. The electrical and optical properties were studied by optical microscopy, impedance and VASE measurements.

From optical microscopy pictures of the samples, it is possible to observe that a color transition from dark yellow to black occurs as a sign of GO reduction.

We found from impedance measurements that the electric resistance of RGO films decreased by about two orders of magnitude in comparison to GO films.

We found from VASE measurements that thermal annealing increased the optical conductivity of GO by about one order of magnitude. In addition, thermal annealing increased the absorption coefficient of GO films.

Hence, the electrical and optical properties of GO films are significantly enhanced using a thermal annealing treatment.

RGO films on glass substrates, obtained using thermal annealing, could thus find use in several fields, such as solar cells and other optoelectronic applications.

Supplementary Materials: The following supporting information can be downloaded at: https://www.mdpi.com/article/10.3390/cryst12091312/s1, Figure S1: Scanning electron microscopy image of GO films on Si/SiO_2 substrates. Figure S2: Scanning electron microscopy image of RGO films on Si/SiO_2 substrates.

Author Contributions: Investigation, G.G.P. and C.V.; Supervision, C.V.; Writing—original draft, G.G.P. and C.V.; Writing—review and editing, G.G.P. and C.V. All authors have read and agreed to the published version of the manuscript.

Funding: This research received no external funding.

Institutional Review Board Statement: Not applicable.

Informed Consent Statement: Not applicable.

Data Availability Statement: Not applicable.

Conflicts of Interest: The authors declare no conflict of interest.

References

1. Sun, Y.; Xia, H. Bi2Te3/Graphene Heterostructure as the Saturable Absorber for ~1.0 μm Passively Q-switched Solid State Pulsed Laser. *Crystals* **2022**, *12*, 222. [CrossRef]
2. Wang, X.; Lu, S.; Xu, W. Synthesis of Needle-like Nanostructure Composite Electrode of Co3O4/rGO/NF for High-Performance Symmetric Supercapacitor. *Crystals* **2022**, *12*, 664. [CrossRef]
3. Zhang, Q.; Pang, X.; Zhao, Y. Effect of the External Velocity on the Exfoliation Properties of Graphene from Amorphous SiO_2 Surface. *Crystals* **2021**, *11*, 454. [CrossRef]
4. Yi, L.; Li, C. Simulation Study of In-Phase and Out-Phase Enhanced Absorption of Graphene Based on Parity–Time Symmetry One-Dimensional Photonic Crystal Structure. *Crystals* **2021**, *11*, 1513. [CrossRef]
5. Liu, N.; Tang, Q.; Huang, B.; Wang, Y. Graphene Synthesis: Method, Exfoliation Mechanism and Large-Scale Production. *Crystals* **2022**, *12*, 25. [CrossRef]
6. El-Sayed, F.; Hussien, M.S.A.; AlAbdulaal, T.H.; Ismail, A.; Zahran, H.Y.; Yahia, I.S.; Abdel-wahab, M.S.; Khairy, Y.; Ali, T.E.; Ibrahim, M.A. Comparative Degradation Studies of Carmine Dye by Photocatalysis and Photoelectrochemical Oxidation Processes in the Presence of Graphene/N-Doped ZnO Nanostructures. *Crystals* **2022**, *12*, 535. [CrossRef]
7. Cai, X.; Sun, K.; Qiu, Y.; Jiao, X. Recent Advances in Graphene and Conductive Polymer Composites for Supercapacitor Electrodes: A Review. *Crystals* **2021**, *11*, 947. [CrossRef]
8. Peng, S.; Zhang, J.; Jin, Z.; Zhang, D.; Shi, J.; Wei, S. Electric-Field Induced Doping Polarity Conversion in Top-Gated Transistor Based on Chemical Vapor Deposition of Graphene. *Crystals* **2022**, *12*, 184. [CrossRef]
9. Zheng, C.; Lu, H.; Xu, Q.; Liu, T.; Patil, A.; Wu, J.; de Vries, R.; Zuilhof, H.; Zhang, Z. Effect of Graphene on Ice Polymorph. *Crystals* **2021**, *11*, 1134. [CrossRef]
10. Alahmed, I.I.; Altanany, S.M.; Abdulazeez, I.; Shoaib, H.; Alsayoud, A.Q.; Abbout, A.; Peng, Q. The Crack Angle of 60° Is the Most Vulnerable Crack Front in Graphene According to MD Simulations. *Crystals* **2021**, *11*, 1355. [CrossRef]
11. Nam, M.H.; Tung, B.S.; Khuyen, B.X.; Ha, D.T.; Ngoc, N.V.; Tran, M.C.; Le, D.T.; Lam, V.D.; Chen, L.; Zheng, H.; et al. Graphene-Integrated Plasmonic Metamaterial for Manipulation of Multi-Band Absorption, Based on Near-Field Coupled Resonators. *Crystals* **2022**, *12*, 525. [CrossRef]
12. Wang, S.; Wang, X.; He, J.; Xin, M. Mechanical Behavior and Microstructure of Graphene Oxide Electrodeposited Carbon Fiber Reinforced Cement-Based Materials. *Crystals* **2022**, *12*, 964. [CrossRef]
13. Shoaib, H.; Peng, Q.; Alsayoud, A.Q. Atomic Insights into Fracture Characteristics of Twisted Tri-Layer Graphene. *Crystals* **2021**, *11*, 1202. [CrossRef]
14. Alshoaibi, A.; Awada, C.; Ahmed, F.; Obodo, R.M.; Maaza, M.; Ezema, F.I. Trimetallic Oxides/GO Composites Optimized with Carbon Ions Radiations for Supercapacitive Electrodes. *Crystals* **2022**, *12*, 874. [CrossRef]
15. Politano, G.G.; Versace, C. Variable Angle Spectroscopic Ellipsometry Characterization of Graphene Oxide in Methanol Films. *Crystals* **2022**, *12*, 696. [CrossRef]
16. Alangari, A.; Aldakheel, F.M.; Mateen, A.; Alqhatani, M.S.; Alaofi, A.L.; Shahid, M.; Ali, R.; Syed, R.; Adil, S.F.; Khan, M.; et al. Assessment of Physicochemical, Anticancer, Antimicrobial, and Biofilm Activities of N-Doped Graphene. *Crystals* **2022**, *12*, 1035. [CrossRef]
17. Zhao, X.; Han, J.; Yang, P.; Zhao, R. Research on High-Efficiency Transmission Characteristics of Multi-Channel Breast Ultrasound Signals Based on Graphene Structure. *Crystals* **2021**, *11*, 507. [CrossRef]
18. Lisovski, O.; Piskunov, S.; Bocharov, D.; Zhukovskii, Y.F.; Kleperis, J.; Knoks, A.; Lesnicenoks, P. CO_2 and CH_2 Adsorption on Copper-Decorated Graphene: Predictions from First Principle Calculations. *Crystals* **2022**, *12*, 194. [CrossRef]
19. Wu, S. Recent Progress in Flexible Graphene-Based Composite Fiber Electrodes for Supercapacitors. *Crystals* **2021**, *11*, 1484. [CrossRef]
20. Wu, X.; Yin, B. Mechanism and Properties of UO_2–Graphene Composite Fuel Prepared by In Situ Synthesis. *Crystals* **2022**, *12*, 230. [CrossRef]
21. Yang, L.; Xiao, W.; Wang, J.; Li, X.; Wang, L. Adsorption and Sensing Properties of Formaldehyde on Chemically Modified Graphene Surfaces. *Crystals* **2022**, *12*, 553. [CrossRef]
22. Handayani, M.; Nafi'ah, N.; Nugroho, A.; Rasyida, A.; Prasetyo, A.B.; Febriana, E.; Sulistiyono, E.; Firdiyono, F. The Development of Graphene/Silica Hybrid Composites: A Review for Their Applications and Challenges. *Crystals* **2021**, *11*, 1337. [CrossRef]
23. Gupta, M.; Hawari, H.F.; Kumar, P.; Burhanudin, Z.A. Copper Oxide/Functionalized Graphene Hybrid Nanostructures for Room Temperature Gas Sensing Applications. *Crystals* **2022**, *12*, 264. [CrossRef]
24. Politano, G.G.; Versace, C. Variable-Angle Spectroscopic Ellipsometry of Graphene-Based Films. *Coatings* **2021**, *11*, 462. [CrossRef]
25. Politano, G.G.; Vena, C.; Desiderio, G.; Versace, C. Variable Angle Spectroscopic Ellipsometry Characterization of Reduced Graphene Oxide Stabilized with Poly (Sodium 4-Styrenesulfonate). *Coatings* **2020**, *10*, 743. [CrossRef]
26. Politano, G.G.; Vena, C.; Desiderio, G.; Versace, C. Variable angle spectroscopic ellipsometry characterization of turbostratic CVD-grown bilayer and trilayer graphene. *Opt. Mater.* **2020**, *107*, 110165. [CrossRef]

27. Politano, G.G.; Nucera, A.; Castriota, M.; Desiderio, G.; Vena, C.; Versace, C. Spectroscopic and morphological study of graphene nanoplatelets thin films on Si/SiO_2 substrates. *Mater. Res. Express* **2019**, *6*, 106432. [CrossRef]
28. Politano, G.G.; Cazzanelli, E.; Versace, C.; Castriota, M.; Desiderio, G.; Davoli, M.; Vena, C.; Bartolino, R. Micro-Raman investigation of Ag/graphene oxide/Au sandwich structure. *Mater. Res. Express* **2019**, *6*, 075605. [CrossRef]
29. Castriota, M.; Politano, G.G.; Vena, C.; de Santo, M.P.; Desiderio, G.; Davoli, M.; Cazzanelli, E.; Versace, C. Variable Angle Spectroscopic Ellipsometry investigation of CVD-grown monolayer graphene. *Appl. Surf. Sci.* **2019**, *467–468*, 213–220. [CrossRef]
30. Wang, J.; Ma, F.; Liang, W.; Sun, M. Electrical properties and applications of graphene, hexagonal boron nitride (h-BN), and graphene/h-BN heterostructures. *Mater. Today Phys.* **2017**, *2*, 6–34. [CrossRef]
31. Cho, S.; Fuhrer, M.S. Charge transport and inhomogeneity near the minimum conductivity point in graphene. *Phys. Rev. B* **2008**, *77*, 81402. [CrossRef]
32. Tan, Y.-W.; Zhang, Y.; Bolotin, K.; Zhao, Y.; Adam, S.; Hwang, E.H.; Sarma, S.D.; Stormer, H.L.; Kim, P. Measurement of Scattering Rate and Minimum Conductivity in Graphene. *Phys. Rev. Lett.* **2007**, *99*, 246803. [CrossRef] [PubMed]
33. Majumder, P.; Gangopadhyay, R. Evolution of graphene oxide (GO)-based nanohybrid materials with diverse compositions: An overview. *RSC Adv.* **2022**, *12*, 5686–5719. [CrossRef] [PubMed]
34. Eda, G.; Fanchini, G.; Chhowalla, M. Large-area ultrathin films of reduced graphene oxide as a transparent and flexible electronic material. *Nat. Nanotechnol.* **2008**, *3*, 270. [CrossRef] [PubMed]
35. Dreyer, D.R.; Park, S.; Bielawski, C.W.; Ruoff, R.S. The chemistry of graphene oxide. *Chem. Soc. Rev.* **2010**, *39*, 228–240. [CrossRef] [PubMed]
36. Moon, I.K.; Lee, J.; Ruoff, R.S.; Lee, H. Reduced graphene oxide by chemical graphitization. *Nat. Commun.* **2010**, *1*, 73. [CrossRef]
37. Bourlinos, A.B.; Gournis, D.; Petridis, D.; Szabó, T.; Szeri, A.; Dékány, I. Graphite Oxide: Chemical Reduction to Graphite and Surface Modification with Primary Aliphatic Amines and Amino Acids. *Langmuir* **2003**, *19*, 6050–6055. [CrossRef]
38. Dai, B.; Fu, L.; Liao, L.; Liu, N.; Yan, K.; Chen, Y.; Liu, Z. High-quality single-layer graphene via reparative reduction of graphene oxide. *Nano Res.* **2011**, *4*, 434–439. [CrossRef]
39. Díez-Betriu, X.; Álvarez-García, S.; Botas, C.; Álvarez, P.; Sánchez-Marcos, J.; Prieto, C.; Menéndez, R.; de Andrés, A. Raman spectroscopy for the study of reduction mechanisms and optimization of conductivity in graphene oxide thin films. *J. Mater. Chem. C* **2013**, *1*, 6905–6912. [CrossRef]
40. Tkachev, S.V.; Buslaeva, E.Y.; Naumkin, A.V.; Kotova, S.L.; Laure, I.V.; Gubin, S.P. Reduced graphene oxide. *Inorg. Mater.* **2012**, *48*, 796–802. [CrossRef]
41. Schöche, S.; Hong, N.; Khorasaninejad, M.; Ambrosio, A.; Orabona, E.; Maddalena, P.; Capasso, F. Optical properties of graphene oxide and reduced graphene oxide determined by spectroscopic ellipsometry. *Appl. Surf. Sci.* **2017**, *421*, 778–782. [CrossRef]
42. Hou, D.; Liu, Q.; Wang, X.; Quan, Y.; Qiao, Z.; Yu, L.; Ding, S. Facile synthesis of graphene via reduction of graphene oxide by artemisinin in ethanol. *J. Mater.* **2018**, *4*, 256–265. [CrossRef]
43. Jung, I.; Dikin, D.A.; Piner, R.D.; Ruoff, R.S. Tunable Electrical Conductivity of Individual Graphene Oxide Sheets Reduced at "Low" Temperatures. *Nano Lett.* **2008**, *8*, 4283–4287. [CrossRef] [PubMed]
44. Hassan, A.A.; Azam, A.; Ahn, M.; Zubair, Y.H.; Cao, M.; Khan, Y. Low Dark Current and Performance Enhanced Perovskite Photodetector by Graphene Oxide as an Interfacial Layer. *Nanomaterials* **2022**, *12*, 190. [CrossRef]
45. Marchezi, P.E.; de Araújo, F.L.; Szostack, R.; Germino, J.C.; Therézio, E.M.; Marletta, A.; Nogueira, A.F. Reduced graphene oxide in perovskite solar cells: The influence on film formation, photophysics, performance, and stability. *J. Mater. Chem. C* **2021**, *9*, 14648–14658. [CrossRef]
46. Loh, K.P.; Bao, Q.; Eda, G.; Chhowalla, M. Graphene oxide as a chemically tunable platform for optical applications. *Nat. Chem.* **2010**, *2*, 1015–1024. [CrossRef]
47. Yin, Z.; Wu, S.; Zhou, X.; Huang, X.; Zhang, Q.; Boey, F.; Zhang, H. Electrochemical Deposition of ZnO Nanorods on Transparent Reduced Graphene Oxide Electrodes for Hybrid Solar Cells. *Small* **2010**, *6*, 307–312. [CrossRef]
48. Jaafar, E.; Kashif, M.; Sahari, S.K.; Ngaini, Z. Study on Morphological, Optical and Electrical Properties of Graphene Oxide (GO) and Reduced Graphene Oxide (rGO). *Mater. Sci. Forum* **2018**, *917*, 112–116. [CrossRef]
49. Jung, I.; Vaupel, M.; Pelton, M.; Piner, R.; Dikin, D.A.; Stankovich, S.; An, J.; Ruoff, R.S. Characterization of Thermally Reduced Graphene Oxide by Imaging Ellipsometry. *J. Phys. Chem. C* **2008**, *112*, 8499–8506. [CrossRef]
50. Shen, Y.; Yang, S.; Zhou, P.; Sun, Q.; Wang, P.; Wan, L.; Li, J.; Chen, L.; Wang, X.; Ding, S.; et al. Evolution of the band-gap and optical properties of graphene oxide with controllable reduction level. *Carbon* **2013**, *62*, 157–164. [CrossRef]
51. Mohandoss, M.; Nelleri, A. Optical properties of sunlight reduced graphene oxide using spectroscopic ellipsometry. *Opt. Mater.* **2018**, *86*, 126–132. [CrossRef]
52. Woollam, J.A.; Johs, B.D.; Herzinger, C.M.; Hilfiker, J.N.; Synowicki, R.A.; Bungay, C.L. Overview of variable-angle spectroscopic ellipsometry (VASE): I. Basic theory and typical applications. *Proc. SPIE* **1999**, *10294*, 3–28.
53. Scriven, L.E. Physics and Applications of DIP Coating and Spin Coating. *MRS Proc.* **1988**, *121*, 717. [CrossRef]
54. Moré, J.J. The Levenberg-Marquardt algorithm: Implementation and theory. In *Numerical Analysis*; Watson, G.A., Ed.; Springer: Berlin/Heidelberg, Germany, 1978; pp. 105–116. [CrossRef]
55. Woollam, J.A. WVASE Manual. In *Guide to Using WVASE32*; J.A. Woollam: Lincoln, NE, USA, 2010.
56. Razaq, A.; Bibi, F.; Zheng, X.; Papadakis, R.; Jafri, S.H.; Li, H. Review on Graphene-, Graphene Oxide-, Reduced Graphene Oxide-Based Flexible Composites: From Fabrication to Applications. *Materials* **2022**, *15*, 1012. [CrossRef]

57. Shen, Y.; Zhou, P.; Sun, Q.Q.; Wan, L.; Li, J.; Chen, L.Y.; Zhang, D.W.; Wang, X.B. Optical investigation of reduced graphene oxide by spectroscopic ellipsometry and the band-gap tuning. *Appl. Phys. Lett.* **2011**, *99*, 141911. [CrossRef]
58. Yakuphanoglu, F.; Sekerci, M.; Ozturk, O.F. The determination of the optical constants of Cu(II) compound having 1-chloro-2,3-o-cyclohexylidinepropane thin film. *Opt. Commun.* **2004**, *239*, 275–280. [CrossRef]